Electronic Supplementary Material (ESI) for RSC Advances.

[Electronic Supplementary Information]

Polypyrrole-decorated CPO-27-M and HKUST-1 metal organic frameworks for supercapacitor devices.

Nigel Patterson,[a] *Bo Xiao,*[*b] *Anna Ignaszak*[*a]

[a]Department of Chemistry, University of New Brunswick, 30 Dineen Drive (Toole Hall), Fredericton, NB, Canada.

[b]School of Chemistry and Chemical Engineering, Queen's University Belfast, Stranmillis Road (David Kier Building), Belfast BT9 5AG, UK.

[*] Corresponding authors:
b.xiao@qub.ac.uk
anna.ignaszak@unb.ca

MOF-conjugated polymer	Specific capacitance	Reference work
PPy-CPO-27-Ni	354 F g^{-1}	This work
PPy-CPO-27-Co	263 F g^{-1}	This work
PPy-HKUST-1	185 F g^{-1}	This work
PPy-CC/ZIF-67	284 F g^{-1}	Dalton Trans. (2018) 47, 13472-13478
PPy-CFs@UiO-66	90 F g^{-1}	ACS Appl. Mater. Interfaces (2018) 10, 18021-18028
NENU-5/PPy-0.15	779 F g^{-1}	ACS Appl. Mater. Interfaces (2018) 10, 32265-32270
PPy-2-ZIF	554 F g^{-1}	ACS Appl. Mater. Interfaces (2018) 10, 38737-38744
PPy-Ni-MOF	715 F g^{-1}	RSC Adv. (2020) 10, 12129-12134
PPy-MIL-51(Al)*	0.51 F cm^{-2}	Electrochimica Acta (2020) 336, 13574 (1-12)
PPy-NiCo-MOF@PNTs	1109 F g^{-1}	Applied Surface Science (2020) 507, 145089 (1-8)
PPy-Cu-CAT-NWAs*	0.252 F cm^{-2}	Adv. Energy Mater. (2020) 10, 1901892 (1-9)
PPy-UiO-66@cotton	565 F g^{-1}	Cellulose (2019) 26, 3387-3399
PANI-Zn-MOF	477 F g^{-1}	J. Power Source (2016) 316, 176-182
PANI-ZIF67-CC	371 F g^{-1}	J. Am. Chem. Soc. (2015) 137, 4920-4923
PANI-CNT@ZIF-67-CC	371 F g^{-1}	Electrochimica Acta (2017) 240, 16-23
PANI-Co-MOF	504 F g^{-1}	Inorganica Chimica Acta (2020) 502, 1193932 (1-11)
PANI-MOF	1268 F g^{-1}	Nanotechnology (2019) 30, 085404 (1-13)
PANI-(ZIF-8, ZIF-67)	89 – 746 F g^{-1}	AIP Advances (2019) 9, 055032 (1-5)
PANI-Cu-MOF	734 F g^{-1}	Journal of Inorganic and Organometallic Polymers and Materials (2019) 29, 1838-1847
Ni-MOF/PANI/NF*	3.6 F cm^{-2}	Dalton Trans. (2019) 48, 4119-4123
PANI-HKUST-1	270 F g^{-1}	Physica E: Low-dimensional Systems and Nanostructures (2018) 99, 16–23
PANI-ZIF-67-CC*	2.1 F cm^{-2}	J. Am. Chem. Soc. (2015) 137, 4920-4923
PEDOT-GO/UiO-66-C*	0.1 F cm^{-2}	ChemistrySelect (2016) 2, 285–289
PEDOT/HKUST-1-CNTF*	0.08 F cm^{-2}	Materials Chemistry and Physics (2016) 179, 166e173167

Table S1: Specific capacitances of various reported supercapacitive MOF composites.

Table S1 summarizes various capacitive electrodes comprising conjugated polymers (including PPy, polyaniline (PANI), and poly(3,4-ethylenedioxythiophene) (PEDOT)), MOFs, and other conducting additives. The C_s stated in this work is within the range of the most performing PPy-MOF electrodes currently studied. Although some outstanding C_s is demonstrated, for example in PPy-NiCo-MOF@PNTs and PPy-Ni-MOF, it is important to keep in mind that in both cases the total conductivity of the electrode is significantly higher than in our system due to the presence of Ni or Ni/Co metal nanoparticles. This unquestionably helps charge transfer within the structure of the MOF and the semiconducting polymer. Higher C_s for the NENU-5/PPy-0.15 system (sans additional metal particles) is related to the redox activity of NENU-5 itself, which ultimately contributes in pseudocapacitance of the electrode. In particular, PMo12 units in the MOF's framework facilitate electron transfer at the Mo^{6+}/Mo^{4+} active centers.

Several other reasons are emphasized when comes to improvement of C_s. One is the microporosity of the MOF which can be problematic when it comes to pore blockage by a coated polymer. On the other hand, ultra-small pores prevent the MOF from dissolving in the electrolyte, which in some cases is taken as an advantage when it comes to the long-term stability of the electrode. Another important contributor to the high C_s of such electrodes are the $\pi - \pi$ conjugations between MOFs and PPy. This is believed to facilitate the polymerization process on the surface of MOFs, resulting in uniformly distributed nanostructured polymer particles, resulting in remarkable improvement of electrochemical performance. In summary, the optimized particle sizes of MOFs vs. size of polymer and well-designed porosity both promote the transport of electrolyte ions that is critical to the mechanism of double-layer and pseudocapacitance.

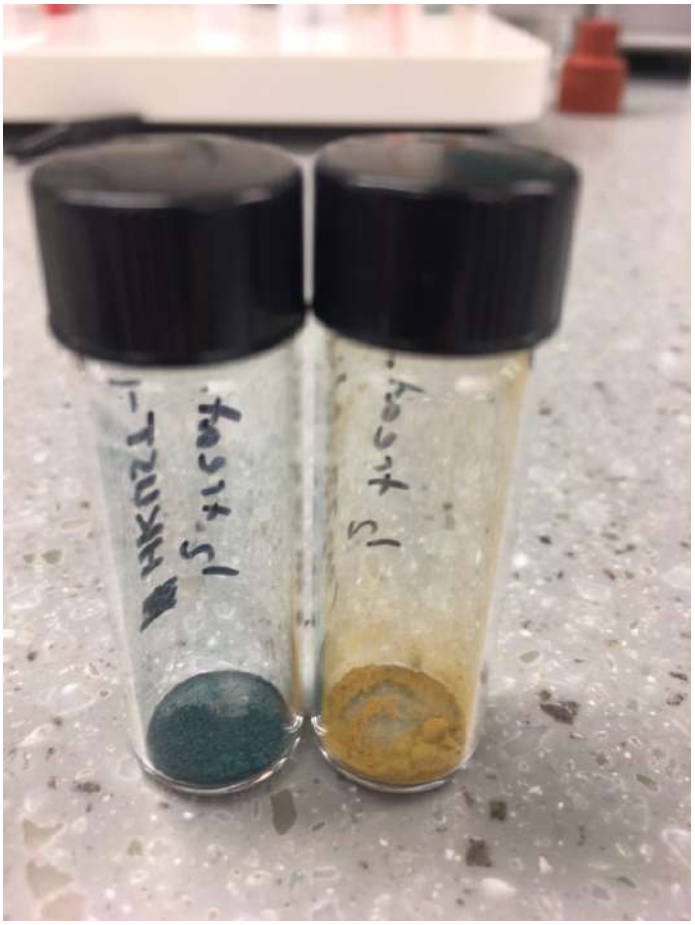

Figure S1: MOFs HKUST-1 (left) and CPO-27-Ni (right) darkened after immersion in iodine

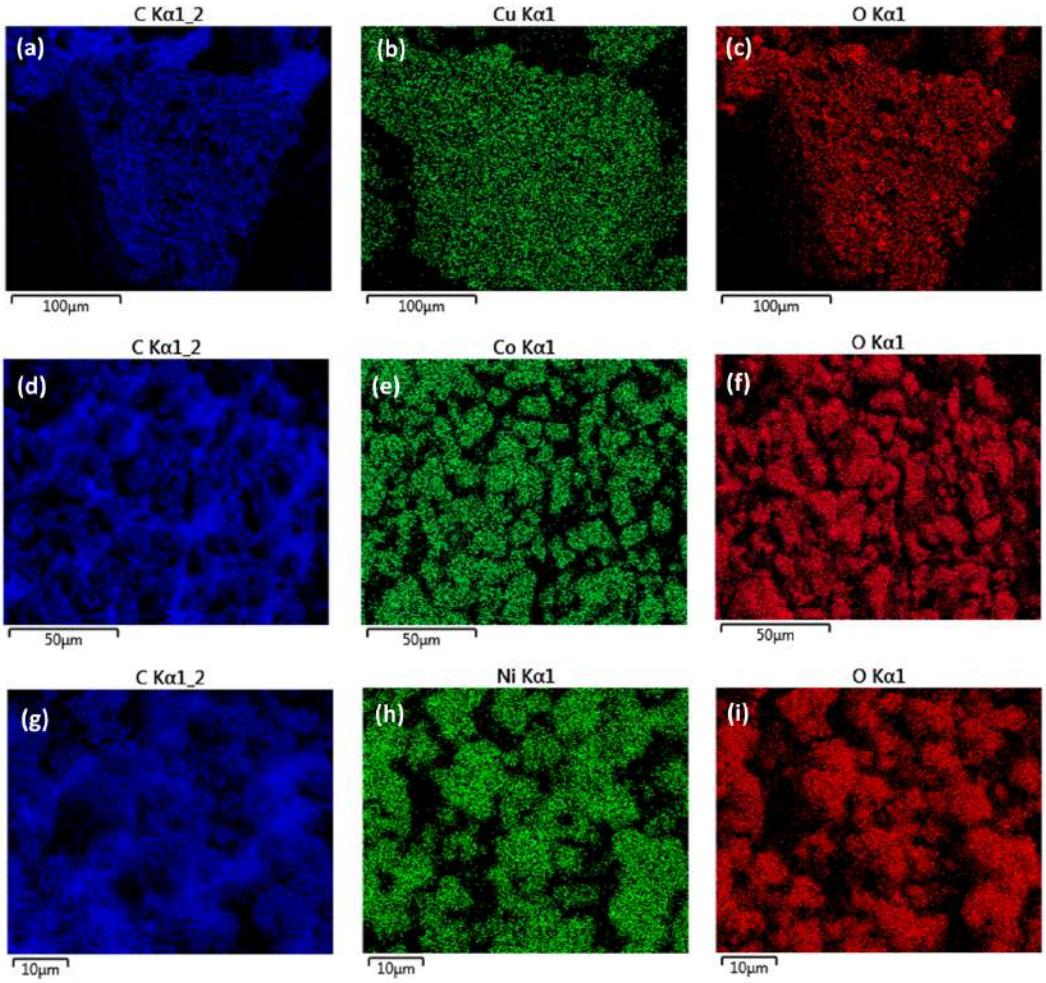

Figure S2: EDS images of PPy-d-MOFs (a,b,c) PPy-HKUST-1, (d,e,f) PPy-CPO-27-Co, (g,h,i) PPy-CPO-27-Ni showing C, O, and metal composition.

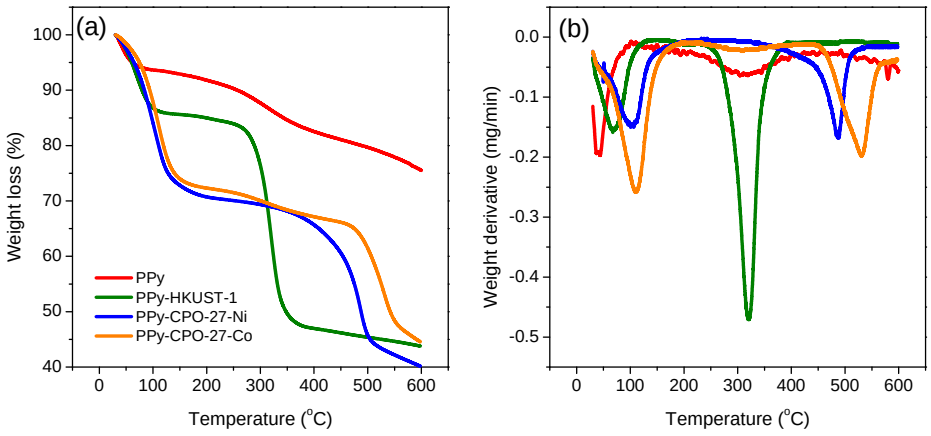

Figure S3: (a) All PPy-d-MOF TGA curves with pure PPy as well. (b) First derivative graphs of the same.

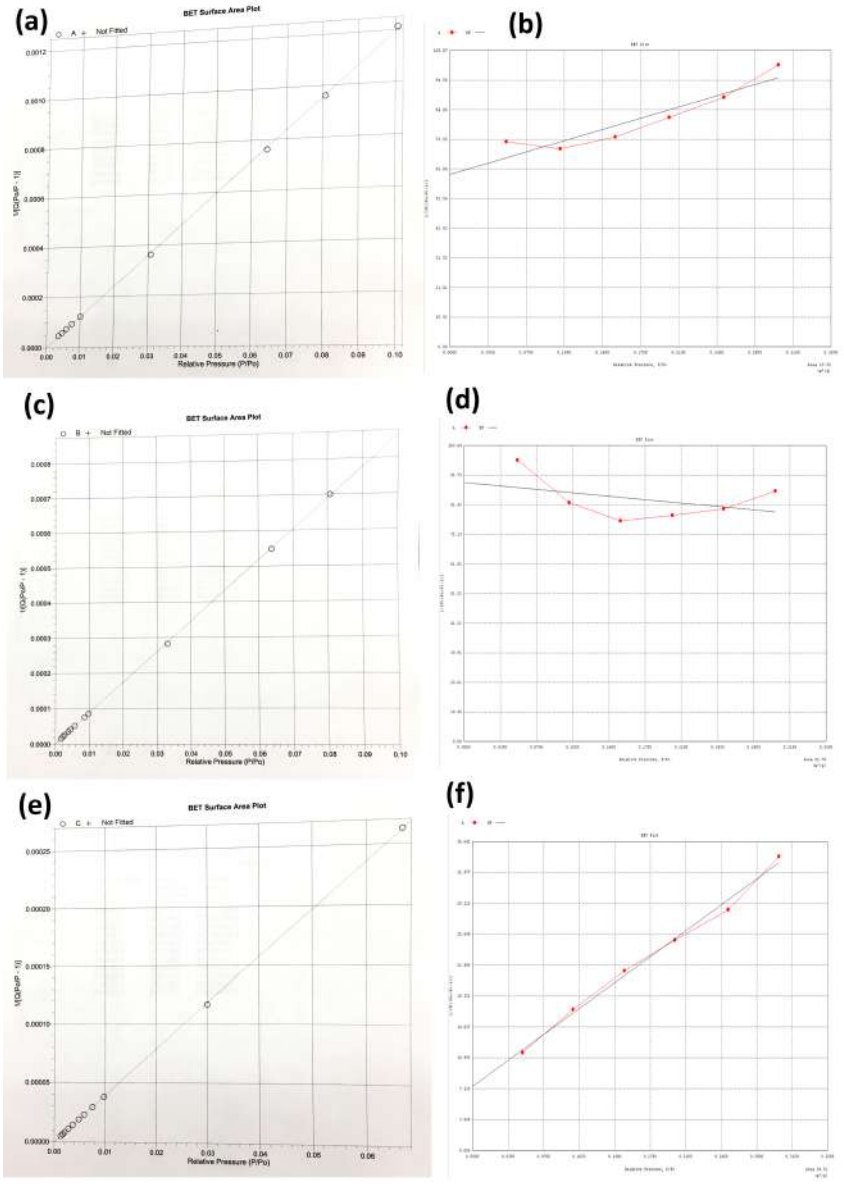

Figure S4: Plots of the BET surface area for (a) CPO-27-Ni, (b) PPy-CPO-27-Ni, (c) CPO-27-Co, (d) PPy-CPO-27-Co, (e) HKUST-1, (f)PPy-HKUST-1.

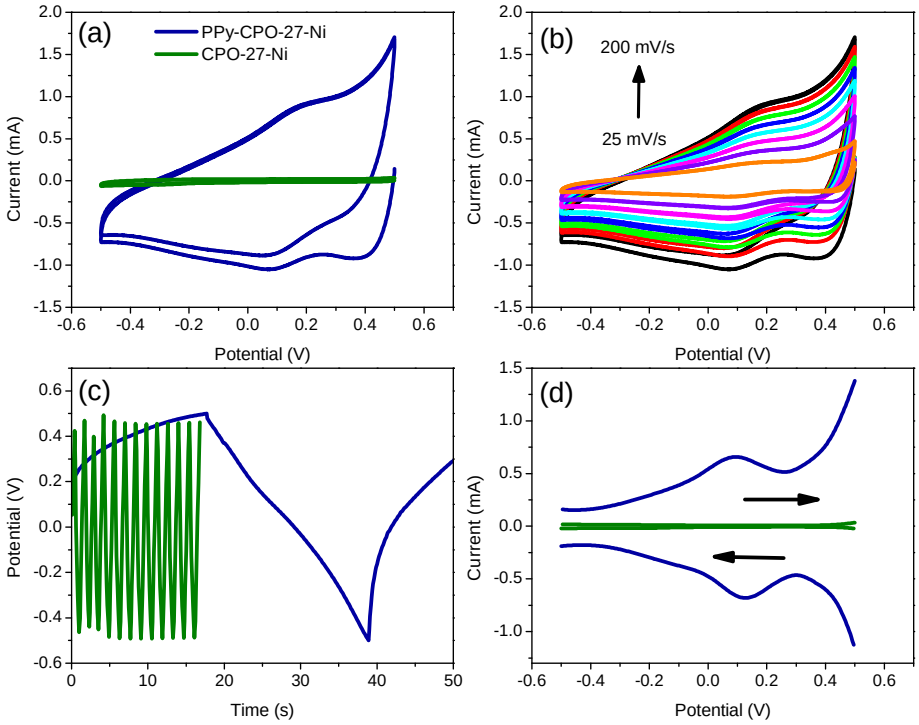

Figure S5: Comparison of plain vs PPy-CPO-27-Ni. (a) CV, (b) CV of just PPy-CPO-27-Ni at varying scan rates, (c) GCD, d) DPV.

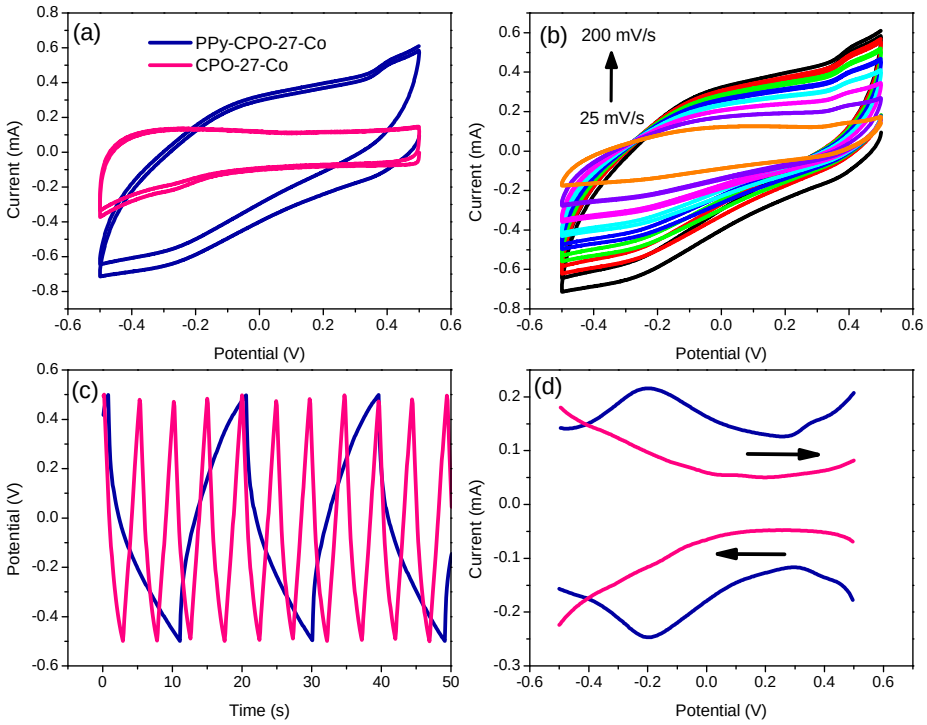

Figure S6: Comparison of plain vs PPy-CPO-27-Co. (a) CV, (b) CV of just PPy-CPO-27-Co at varying scan rates, (c) GCD, d) DPV.

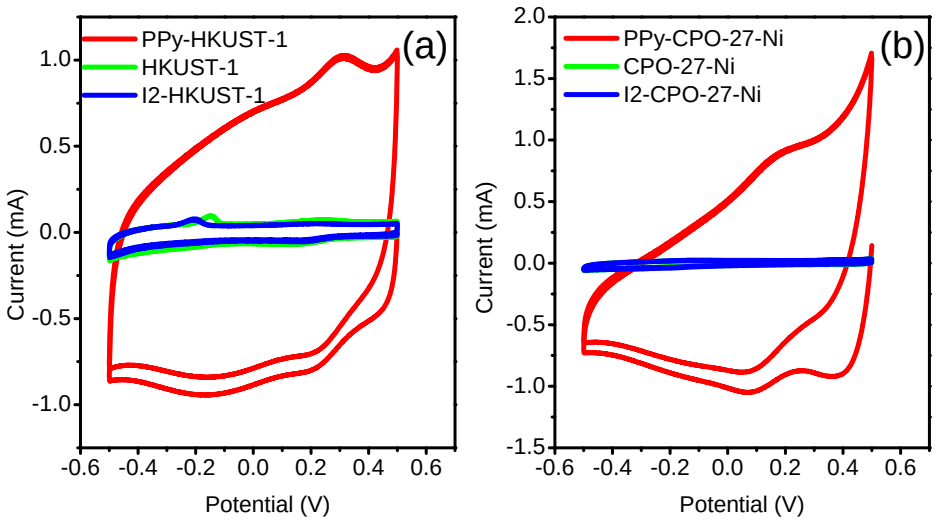

Figure S7: Contribution of plain MOF or I_2-doped MOF (a) HKUST-1, (b) CPO-27-M to overall supercapacitance in PPy-d-MOFs.

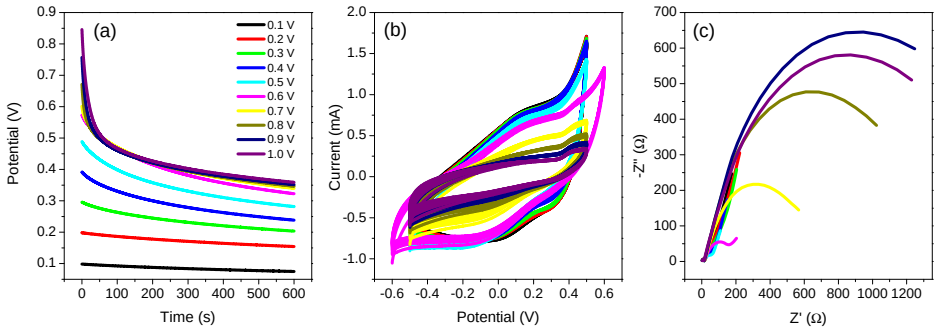

Figure S8: Behaviour of PPy-CPO-27-Ni after successive charging at different potentials. (a) OCP, (b) CV, (c) EIS.

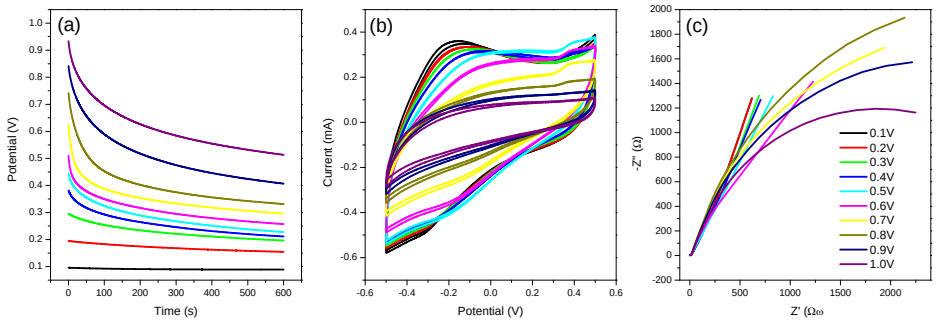

Figure S9: Behaviour of PPy-CPO-27-Co after successive charging at different potentials. (a) OCP, (b) CV, (c) EIS.

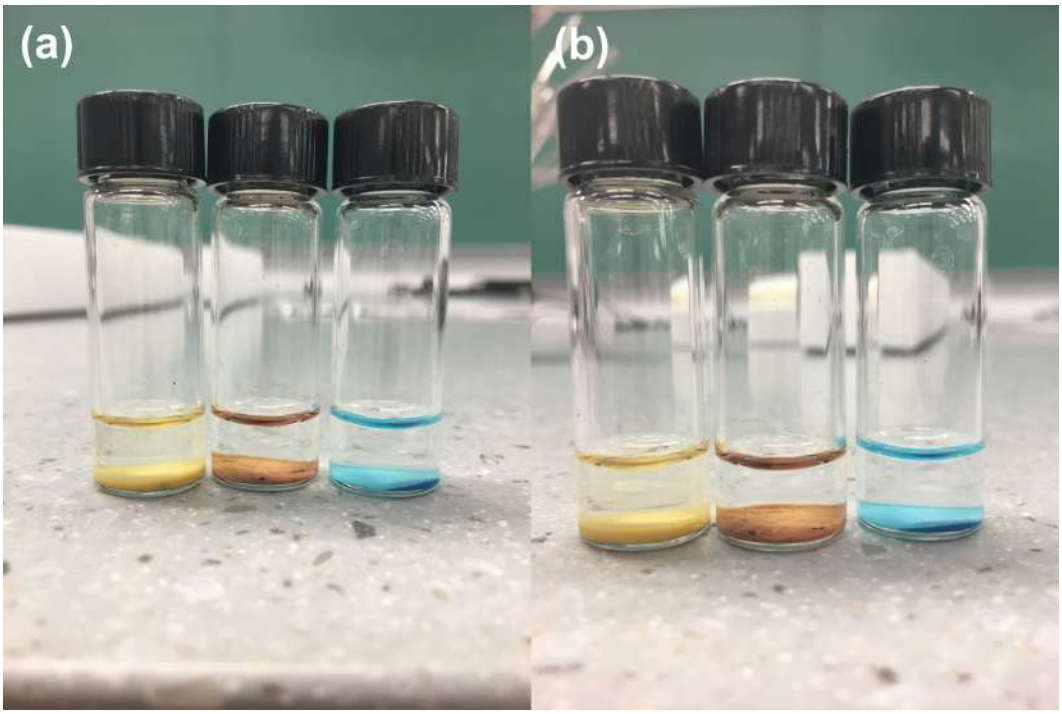

Figure S10: Stability of MOFs in ink (a) initial, (b) after 48 hours, evidenced by lack of discolouration of ink indicating leaching of metals/compounds.